The Astrophysical Journal, 850:54 (8pp), 2017 November 20 https://doi.org/10.3847/1538-4357/aa93dc

ALMA CO(3-2) Observations of Star-forming Filaments in a Gas-poor Dwarf Spheroidal Galaxy

S. Michelle Consiglio[1], Jean L. Turner[1], Sara Beck[2], David S. Meier[3,4], Sergiy Silich[5], and Jun-Hui Zhao[6]
[1] Department of Physics and Astronomy, University of California, Los Angeles, Los Angeles, CA 90095, USA; smconsiglio@ucla.edu
[2] School of Physics and Astronomy, Tel Aviv University, Ramat Aviv, Israel
[3] Department of Physics, New Mexico Institute of Mining and Technology, Socorro, NM 87801, USA
[4] National Radio Astronomy Observatory, Soccorro, NM 87801, USA
[5] Instituto Nacional de Astrofísica, Óptica y Electrónica, Puebla, México 72840, México
[6] Harvard-Smithsonian Center for Astrophysics, Cambridge, MA 02138, USA
Received 2017 April 25; revised 2017 October 2; accepted 2017 October 12; published 2017 November 16

Abstract

We report ALMA observations of ^{12}CO(3-2) and ^{13}CO(3-2) in the gas-poor dwarf galaxy NGC 5253. These 0.″3 (5.5 pc) resolution images reveal small, dense molecular gas clouds that are located in kinematically distinct extended filaments. Some of the filaments appear to be falling into the galaxy and may be fueling its current star formation. The most intense CO(3–2) emission comes from the central ∼100 pc region centered on the luminous radio-infrared H II region known as the supernebula. The CO(3–2) clumps within the starburst region are anti-correlated with Hα on ∼5 pc scales, but are well-correlated with radio free–free emission. Cloud D1, which enshrouds the supernebula, has a high ^{12}CO/^{13}CO ratio, as does another cloud within the central 100 pc starburst region, possibly because the clouds are hot. CO(3–2) emission alone does not allow determination of cloud masses as molecular gas temperature and column density are degenerate at the observed brightness, unless combined with other lines such as ^{13}CO.

Key words: galaxies: dwarf – galaxies: individual (NGC 5253) – galaxies: starburst – galaxies: star clusters: general – submillimeter: galaxies

1. Introduction

Super star clusters (SSCs) are the birth places of most massive stars; these immense concentrations of hot stars have the potential to have an enormous impact on their host galaxies. Understanding the formation and evolution of SSCs is critical to understanding the energy budget, feedback, and regulation of star formation in galaxies and the environments that produce them.

NGC 5253 is a local ($D = 3.8$ Mpc; Sakai et al. 2004) dwarf spheroidal galaxy undergoing an intense starburst that has created a large population of massive star clusters over the course of a Gyr (Meurer et al. 1995; Gorjian 1996; Calzetti et al. 1997, 2004, 2015; Tremonti et al. 2001; Alonso-Herrero et al. 2004; Cresci et al. 2005; Martín-Hernández et al. 2005; de Grijs et al. 2013; Smith et al. 2016). NGC 5253 has a stellar mass of only $\sim 1.5 \times 10^8\ M_\odot$ (Martin 1998), and a dark matter mass that is likely 8–9 times higher (Mac Low & Ferrara 1999). This is a galaxy with dispersion-dominated kinematics and little rotation (Atherton et al. 1982; Caldwell & Phillips 1989). The abundant atomic hydrogen gas, comparable to the stellar mass at $\sim(2\text{–}3) \times 10^8\ M_\odot$ (Kobulnicky & Skillman 1995, 2008; López-Sánchez et al. 2012), resides largely outside the galaxy, in filaments and streamers extending to ∼3–5 kpc (∼2–3 optical radii).

The dominant radio/IR H II region in NGC 5253, the supernebula, is excited by a massive, young SSC (Turner et al. 2000; Gorjian et al. 2001; Meier et al. 2002; Turner & Beck 2004). The supernebula has an ionizing rate of $N_{\rm Lyc} = 3.3 \times 10^{52}\ {\rm s}^{-1}$ (Turner et al. 2015; Bendo et al. 2017 corrected for dust following Inoue 2001), corresponding to an IR luminosity of $\sim 5 \times 10^8\ L_\odot$ (Gorjian et al. 2001), contributing to a total galactic infrared luminosity of $1.6 \times 10^9\ L_\odot$ (Vanzi & Sauvage 2004; Hunt et al. 2005). Many investigators find that there are two massive clusters in the nucleus (e.g., Alonso-Herrero et al. 2004; Calzetti et al. 2015), one associated with the supernebula and one associated with the Hα peak; however, extinction within the central starburst region is very high, making it difficult to match radio, infrared, and optical observations (Calzetti et al. 1997; Turner et al. 2003; Martín-Hernández et al. 2005). Abundant molecular gas associated with such a luminous H II region in the ultracompact stage is expected, but the CO(1-0) and (2-1) emission is weak. Roughly three-quarters of this CO emission, as well as the H I, is found along the minor axis, outside the central regions (Turner et al. 1997; Meier et al. 2002; Miura et al. 2015).

Previous observations of CO(3–2) from the Submillimeter Array (SMA) indicate that the star formation in the CO cloud (Cloud D) near the supernebula is very efficient, having converted >50% of its gas mass into stars (Turner et al. 2015). The unexpectedly bright CO(3–2) emission in the central starburst region, as compared to lower J CO lines, indicates that this central cloud, Cloud D (Meier et al. 2002), is warm, $T \sim 300$ K. However, the $\sim 4'' \times 2''$ beam of the SMA images does not separate the dense gas at the cluster scale.

With higher resolution and sensitivity, the Atacama Large Millimeter/Submillimeter Array (ALMA) can image NGC 5253 at the ∼5 pc cluster scale. We have been able to image the structure of its remarkable starburst. Here we present 2015 ALMA observations of the $J = 3$–2 rotational transition of CO in NGC 5253 with 0.″3 (∼5.5 pc) resolution.

2. Observations

NGC 5253 was observed in ALMA Band 7 as a Cycle 1 (Early Science) program executed in Cycle 2 (ID = 2012.1.00105.S: PI = J. Turner) on 2015 June 4 and 5. Two fields, each with

an 18″ field-of-view centered on 13:39:56.62–31.38.33.5 and 13:39:55.91–31.38.26.5 (ICRS), were observed simultaneously with 8383 seconds on both sources. The uv range covers ∼24.5–900 kλ; the largest structures sampled are 4″–8″. Spectral resolution of 244.14 kHz, or 1 km s^{-1} per channel, resolves the CO(3–2) lines. Bandpass, flux, and phase were calibrated with J1427-42064, Titan, and J1342-2900, respectively. Absolute flux density calibration is estimated to be better than 10% in Band 7 Cycle 2 (Lundgren et al. 2013). Data calibration was performed using the code produced by the Joint ALMA Observatories with Common Astronomy Software Applications (CASA). Continuum emission was subtracted in the (u, v) plane before creating the line maps. The beam size is 0.″33 × 0.″27 at p.a. = −89.°8 for ^{12}CO (3–2) and 0.″33 × 0.″29 at p.a. = 89.°0 for ^{13}CO(3–2). The conversion to brightness is such that 1 K corresponds to ∼10–17 mJy, depending on the source geometry. The rms in a single 1 km s^{-1} channel is 2.7 mJy/bm for ^{12}CO(3-2) and 3.2 mJy/bm for ^{13}CO. Integrated intensity images (MOM0) were created by summing up all of the emission that was greater than $\pm 1\sigma$ in all of the channels; for the intensity-weighted mean velocity map (MOM1) the cutoff was $\pm 5\sigma$.

The single dish integrated flux density reported by Meier et al. (2001) with the 22″ CSO beam was 3.4 K km s^{-1}, corresponding to ∼155–170 Jy km s^{-1}, depending on the assumed source geometry. The integrated flux density recovered in the lower resolution SMA synthesis map of Turner et al. (2015) was 110 ± 20 Jy km s^{-1}. We detect ≈50% of the expected integrated flux density from the SMA maps in the form of individual clumps; the remaining flux density is extended and much has been resolved out because of the lack of short spacings in the array. Although the individual dense clouds that emit CO(3-2) are not likely to be large, collections of such clouds with low ($\lesssim$10%) volume filling may lie below even the ALMA sensitivity limit.

3. The ^{12}CO(3–2) Line: How is the Dense Gas in NGC 5253 Distributed?

3.1. The Dense Gas is Clumpy and the Clumps Form Filaments

The CO(3-2) integrated line intensity, $S_{\rm CO} = \int I_{\rm CO} dv$, in NGC 5253 is shown in Figure 1, superimposed on an archival *Hubble Space Telescope*/Advanced Camera for Surveys (*HST*/ACS) image of the galaxy. The $J = 3$ state of CO has an excitation energy of 33 K, requiring a critical density of $n \gtrsim 20{,}000$ cm^{-3} for excitation, thus the $J = 3$ state of CO tends to trace warm and dense star-forming molecular clouds (Heiderman et al. 2010; Lada et al. 2010).

Within the ∼30″ by 60″ region covered by the two ALMA pointings, CO is detected over an area ≈20″ or 370 pc. We identify five regions, labeled in Figure 2, whose properties are given in Table 1. In addition to Cloud D (Meier et al. 2002; Turner et al. 2015), which has the brightest CO(3–2) clumps, there is the Streamer, which lies along the optical dust lane to the southeast, Cloud E, as observed in Meier et al. (2002), northwest of the center, Cloud F from Turner et al. (2015) to the southwest, and finally, the Southern filament, a group of clumps due south of the center. Individual filaments have characteristic widths of only a few clumps, ∼0.″5, but typical lengths of ∼5″ or 90 pc. Individual clumps at these densities have gravitational collapse free-fall timescales of $t_{ff} \lesssim 3.6 \times 10^5$ years.

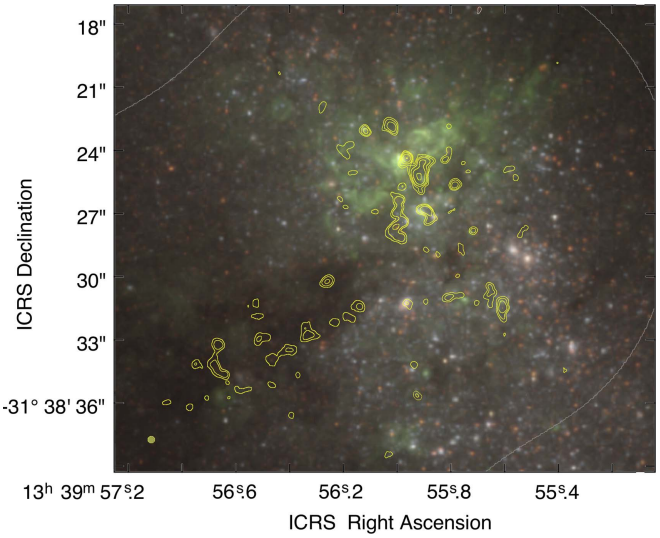

Figure 1. ALMA CO(3-2) contours are overlaid on an archival *HST*/ACS image of NGC 5253 in the 814W, 555W, and 435W bands in red, green, and blue channels, respectively, showing the stars. Contours are $2^n \times 0.1$ Jy bm^{-1} km s^{-1}. CO(3–2) falls along the dust lanes. Registration is estimated to be better than 0.″3, determined by aligning the supernebula/Cloud D1 with the infrared nebula (Turner et al. 2017; D. Cohen et al. 2017, in preparation). The half power of the primary beams of the two mosaicked pointings (field-of view) outlined at the edges of the figure. The ALMA beam is 0.″33 × 0.″27, p.a. = −89.°8, shown in the bottom left.

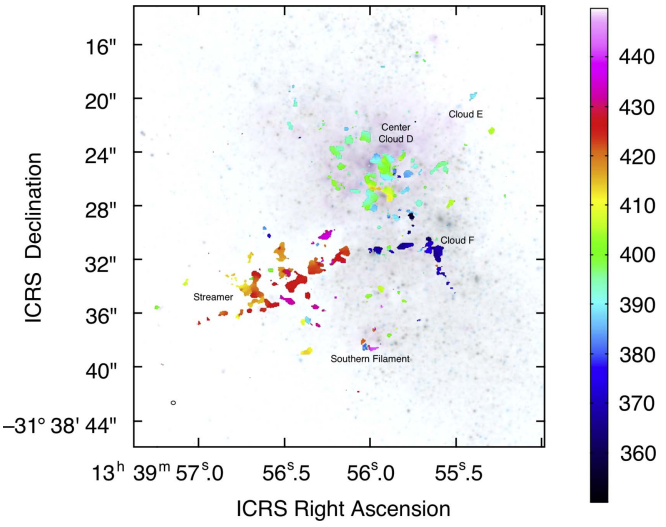

Figure 2. Intensity-weighted mean velocity, MOM1, image of CO(3–2) in NGC 5253. Regions and filaments discussed in the text are labeled; the velocity scale, barycentric, is shown at right. The MOM1 map is constructed from emission >5σ in absolute value. It is shown superposed on an *HST* F555W image. The figure shows that the filamentary structures that appear in the integrated intensity map of Figure 1 are also distinct kinematically. The ALMA beam is shown in the bottom left.

Previous observations of NGC 5253 established that lower J CO emission is located primarily in the Streamer (Turner et al. 1997; Meier et al. 2002; Miura et al. 2015; Turner et al. 2015), following the prominent dust lane to the east along the minor axis of the galaxy. Optical emission lines, probably from the surface of the streamer, are also present in this feature (Graham 1981; Martin 1998; Zastrow et al. 2011). At the 10 times higher spatial resolution of the ALMA images, the Streamer splits up into clumps roughly a beam size (∼0.″3,

Table 1
Source ^{12}CO and ^{13}CO Fluxes, Ratio, and Masses

Source	ICRS R.A.[a] 13^h39^m	ICRS Decl.[a] $-31°38'$	v_{sys}[b] (km s^{-1})	^{12}CO(3-2)[c] (Jy km s^{-1})	^{13}CO(3-2)[c] (Jy km s^{-1})	$\frac{^{12}CO}{^{13}CO}$ ratio	^{12}CO Mass[d] (10^3 $M_\odot$)	^{13}CO Mass[e] (10^3 $M_\odot$)
D1	55.965	24.36	385	2.4	0.06 ± 0.05	40^{+30}_{-20}	100	3.0
D2	56.12	23.1	394	0.8	0.07 ± 0.02	12 ± 4	33	0.6
D3	56.03	22.9	395	1.7	0.28 ± 0.04	6 ± 1	70	2.6
D4	55.91	25.0	402	8.4	1.2 ± 0.07	7 ± 0.4	345	11
D5	55.79	25.6	384	0.87	0.12 ± 0.02	7 ± 1	36	1.1
D6	55.88	27.0	409	1.8	0.25 ± 0.04	7 ± 1	74	2.3
Squiggle (D7)	56.0	27	403	4.1	0.5 ± 0.1	9 ± 2	170	4.4
Center Sum of D Clouds	55.95	25	385	20	2.4 ± 0.1	8 ± 0.5	823	24.7
Streamer[f]	56.5	33	430	8.79	0.86 ± 0.2	10 ± 2	360	8.1
Cloud E	55.5	19	400	12.55	0.8 ± 0.2	16 ± 4	510	7.5
Cloud F	55.8	31	368	6.82	0.9 ± 0.1	8 ± 1	280	8.2
Southern Filament	55.9	367	413	2.45	0.54 ± 0.1	5 ± 1	100	5.1
Overall Sum	56.3	30	380	51	5.5	9	2073	53.6

Notes. All measurements are made from velocity-selected, primary beam corrected MOM0 integrated flux density maps. As ^{13}CO emission is weak, ^{12}CO was used to define the velocity regions for each cloud, and all flux was summed up for that velocity range.
[a] Precision in coordinates depends on the compactness and structure of the source.
[b] ±5 km s^{-1}.
[c] Uncertainties in ^{12}CO flux density are 10% from flux density calibration uncertainties unless otherwise stated. Uncertainties in ^{13}CO flux density, which is mostly signal-to-noise limited, are computed from the individual channel rms times $\sqrt{N_{chan}N_{beam}}$.
[d] Mass derived assuming optically thick emission, using a conversion factor of $\alpha_{CO} = 4.7 \times 10^{20}$ cm^{-2} (K kms^{-1})$^{-1}$, and an estimated CO(3–2)/CO(1–0) ratio of 7. This mass will overestimate the cloud mass for optically thin, warm clouds and for clouds in which enclosed stellar mass is significant. Mass includes He.
[e] Mass derived assuming optically thin ^{13}CO flux density and 20 K, a Galactic value of $[CO]/[H_2] = 8.5 \times 10^{-5}$ and an isotopic ratio of 40, except for Cloud D1, where $T = 300$ K is assumed. The Rayleigh–Jeans approximation is not used. This mass will underestimate the true cloud mass for optically thick emission or if the clouds are warmer than 20 K. Mass includes He.
[f] All integrated line intensities, particularly ^{12}CO, are subject to the missing short spacing data, and therefore this image is unable to reconstruct structures >4″ in size This will not affect small clouds such as the Cloud D individual clumps. The Streamer, however, appears to be missing flux on the whole. See the text.

5 pc) in extent or less, arranged in filamentary structures that are ∼25–200 pc in extent.

The properties and kinematics of the clumps within the filaments are discussed in this section. Individual clouds in the central starburst region, within Cloud D, are discussed further in Section 5.

3.2. The Clumps Form Filamentary Structures that are Distinct in Velocity

Kinematic information is important in interpreting the molecular gas structure in NGC 5253. The systemic velocity of the galaxy is not well defined. H I observations show a systemic velocity of ∼400 km s^{-1} (Koribalski et al. 2004). However, H I lies in the outskirts of the galaxy, is asymmetric, and is affected by large infalling streamers (Kobulnicky & Skillman 1995, 2008; López-Sánchez et al. 2012). The Hα images of Atherton et al. (1982) show a central velocity of ∼385 km s^{-1}. Since Hα is more closely associated with the stellar distribution, this is probably closer to the systemic velocity. Our ALMA CO(3–2) intensity-weighted mean velocity (MOM1) image is shown in Figure 2. This image reveals that the median CO radial (radio definition, barycentric) velocity within the central 100 pc is ∼380 km s^{-1}. We adopt 380 km s^{-1} as the central velocity, although it is not clear how our v_{sys} relates to the stellar velocity.

The filamentary structures identified in the integrated intensity image are not only spatially, but kinematically distinct. The Streamer consistently runs ∼40–20 km s^{-1} redward of the systemic velocity v_{sys} ∼ 380 km s^{-1}. Cloud F is ∼ 20–30 km s^{-1} blueward, and the Southern filament is ∼50 km s^{-1} to the red. Clouds D, in the central region, and E are closer to the systemic velocity. Thus, each filament is distinctly defined kinematically and spatially, and formed of gas that is sufficiently dense for the formation of stars. The H I cloud surrounding NGC 5253 is also composed of filaments. The CO filaments of the Streamer have been identified as forming the inner portion of H I filaments (Kobulnicky & Skillman 2008). The other CO(3–2) filaments may also form the inner portion of more extended H I filaments.

Based on radial velocity alone, it cannot be determined if red or blueshifted emission is inflowing or outflowing. However, many of the filaments correspond to areas of extinction in visible images, indicating that they are located on the near side of the galaxy. Since both the Streamer and the Southern filament are redshifted and in the foreground, they are thus falling toward NGC 5253. On this basis, it has previously been proposed that the starburst in NGC 5253 has been fueled by accretion from this dust lane (Turner et al. 1997; Meier et al. 2002).

By contrast Cloud F to the southwest of the central starburst is blueshifted. Cloud F does not lie in an area of obvious extinction. Thus, we propose that Cloud F represents an infalling filament on the far side of the galaxy.

There is no clear velocity structure within individual filaments, which seem to have coherent velocities. In particular, we find no evidence of acceleration in the gas along the

Streamer, as would be expected if it were in free-fall toward the galaxy. Simple models of gravitational free-fall, assuming a centrally concentrated mass structure, predict acceleration of the gas toward the center that is not clearly visible in the data shown in Figure 2. The lack of evidence for acceleration was also noted by Kobulnicky & Skillman (2008) in the associated H I filament. We note, however, that the gas could be infalling nonetheless. Gas experiencing drag can fall toward a central mass at a constant velocity.

3.3. Conditions in the Filament Clumps

The clumps typically have diameters of about a beam, $\lesssim$5 pc, with ^{12}CO(3–2) integrated line intensities of 0.1–0.5 Jy km s^{-1}. Clumps have been individually identified using cprops, a clump finding code designed to identify clumps using velocity and spatial information (Rosolowsky & Leroy 2006). Their individual characteristics will be published elsewhere (S. M. Consiglio et al. 2017, in preparation). Masses for the larger clumps and features are listed in Table 1. To obtain clump masses from the CO emission, we use the CO conversion factor, $X_{\rm CO}$, which relates CO(1–0) integrated line intensities to H_2 gas masses. CO(1–0) is very weak in NGC 5253 (Turner et al. 1997). Thus, CO(1–0) integrated line intensities are estimated from the CO(3–2) using the line ratio, $R_{31} = \frac{I_{\rm CO32}}{I_{\rm CO10}} = 7$, observed in II Zw 40 (Consiglio et al. 2016), a similar low-metallicity star-forming galaxy. The II Zw 40 value is appropriate since the deep ALMA CO(3–2) and CO(1–0) images used for that calculation had matching beams of $\sim$0.″3, similar to the beam here, in a galaxy with a similar enrichment and metallicity environment. This ratio corresponds to optically thick, slightly subthermal gas. However, the unknown value of R_{31} in NGC 5253 is a source of systematic uncertainty in the gas masses. For a conversion factor of $X_{\rm CO} = 4.7 \times 10^{20}$ cm^{-2} (K km s^{-1})$^{-1}$, the CO(3–2) integrated line intensities correspond to clump masses of (3.3–35) $\times$ 10^4 $M_\odot$ (the largest clumps are listed in Table 1). The conversion factor mass may overestimate the masses in Clouds D1 and D2, which are likely to contain significant stellar mass (see the discussion in Sections 5; Turner et al. 2017). These individual dense clumps by themselves are not large enough to form the large ($\sim 10^4 - 10^6\ M_\odot$) clusters that are currently seen in NGC 5253 (de Grijs et al. 2013; Calzetti et al. 2015).

We estimate that individual clouds in the filaments have internal pressures $P/k = nT \gtrsim$ (2–4) $\times$ 10^5 cm^{-3} K for temperatures of $\sim$20 K, and higher for Cloud D, which appears to be warmer. This value is higher than those of typical ambient pressures in the interstellar medium, $P/k = 2250$ cm^{-3} K (Wolfire et al. 2003), of our Galaxy.

4. Dense Gas and Star Formation in NGC 5253

The central $\sim$150 pc region surrounding the supernebula in NGC 5253 (Cloud D of Meier et al. 2002) contains an extraordinary concentration of young stars. Here we use ALMA CO(3-2) images and previous lower resolution observations of CO(2–1) and CO(3–2) to understand the properties of dense gas and related star formation.

The CO(3–2) integrated line intensity is shown with two tracers of star formation, Hα and radio continuum, in Figures 3 and 4. The CO(3–2) clumps in the ALMA image and the Hα emission in NGC 5253 do not show an obvious correlation (Figure 3). In fact on $\sim$5 pc scales these properties appear to be anti-correlated, with CO(3–2) appearing in dust lanes in the Hα image. The correspondence of CO with dust lanes is not surprising: CO forms at $A_V \gtrsim 2$ (e.g., Bisbas et al. 2015), corresponding to an overall cloud column of $A_V \gtrsim 4$. The bright central H II region for which NGC 5253 is so well known (Burbidge & Burbidge 1962) is centered on the heavily extincted supernebula (Turner et al. 2003; Alonso-Herrero et al. 2004; Turner & Beck 2004). Loops and arcs in the Hα suggest that the supernebula is responsible for not only the large scale leakage of photons, but also possibly for winds. Both effects suggest patchiness of extinction in the supernebula

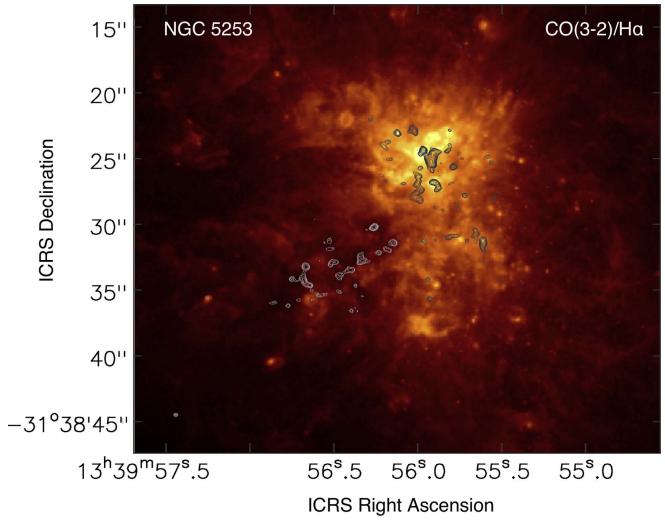

Figure 3. ALMA CO(3-2) image and Hα. The CO(3-2) contours overlaid on an archival *HST* image of Hα emission in color. Contours are $2^{n/2}$ times 80 mJy bm^{-1} km s^{-1}. The CO(3-2) clumps are generally anti-correlated with the Hα, consistent with the $A_V \gtrsim 4$ expected for the clumps. ALMA beam, 0.″33 $\times$ 0.″27, p.a. = −89.°8, is shown in the bottom left.

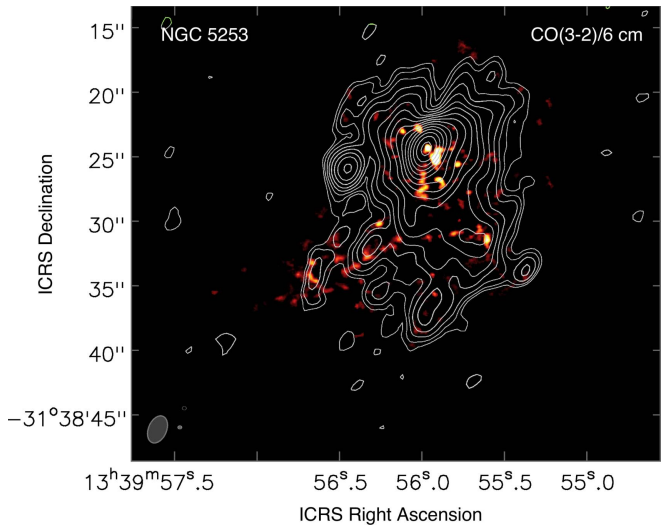

Figure 4. ALMA CO(3-2) image and 6 cm continuum emission. The CO(3-2) is shown in color, over the integrated intensity range of $\sim$0.015 − 4.2 Jy/bm km s^{-1}. The VLA 6 cm emission is contoured at levels of $\pm$0.07 $\times$ $2^{n/2}$ mJy/bm (from Turner et al. 1998). The VLA beam is $\sim$2″, which is much larger than that of the ALMA CO(3-2) beam of $\sim$0.″3; both beams are shown in the lower left. Nearly all the 6 cm emission is thermal free–free emission from the H II regions, which in the absence of extinction, will look like Hα. The exception is that the strong continuum point source at R. A. $\approx$ 56.^{s}5 to the east of the central source is a supernova remnant (Turner et al. 1998).

core, consistent with the kinematics and brightness of Cloud D1 (Turner et al. 2017).

Radio continuum emission traces ionizing photons through free–free emission; like Hα, it traces emission measure, but is far weaker than Hα. Radio continuum is the most reliable tracer of star formation in regions of high extinction. In Figure 4, a VLA 6 cm image (Turner et al. 1998) is overlaid on the ALMA CO(3–2) map. Except for an isolated supernova remnant to the east, the remaining 6 cm emission is thermal free–free emission from the H II regions. The ∼2″ resolution of this VLA image is much lower than the ALMA images, but an excellent spatial correlation of the free–free continuum with CO(3–2) is apparent. The dominant radio continuum source in this image is the supernebula, associated with Cloud D1. Radio continuum peaks are also associated with Cloud F and the Southern Filament, located ∼140–180 pc to the southwest of the supernebula, as well as clouds to the northwest within the Cloud D supernebula complex. The Streamer also shows radio continuum emission, presumably from the same gas producing the "ionization cone" seen in [O III] λ5007, Hα, [S II], and [S III] λλ6716, 9069 (Graham 1981; Martin 1998; Zastrow et al. 2011).

The relation of gas, star formation, and molecular gas depletion time can be estimated from the radio continuum and CO(3–2). Because free–free emission is weak and difficult to detect at subarcsecond scales, we quantify the relation of the 6 cm free–free and CO using the VLA maps with larger 1″–2″ (20–40 pc) beams (Turner et al. 1998) and images of CO(2–1) from the Owens Valley Millimeter (OVRO) Array (Meier et al. 2002) for gas masses. The Streamer has the brightest emission in low J CO images, and contains most of the molecular mass in NGC 5253. The estimated gas mass of the streamer based on CO(2-1) is $\sim 1.7 \times 10^6\ M_\odot$ (corresponding to Cloud C of Meier et al. 2002, corrected to $X_{\rm CO} = 4.7 \times 10^{20}\ {\rm cm^{-2}\ (K\ km^{-1})^{-1}}$). The gas surface density based on their 9.″6×4.″8 beam is $\sim 90\ M_\odot\ {\rm pc^{-2}}$, comparable to the surface densities inferred for giant molecular clouds (GMCs) in the galaxy (Lombardi et al. 2010). Using Starburst 99 models and a full Kroupa initial mass function (IMF), the relation between the young stellar mass and the Lyman continuum rate is $\log[(M/M_\odot)/(N_{\rm Lyc}/{\rm s^{-1}})] = -46.6$, with $N_{\rm Lyc} = 1.25 \times 10^{50}\ {\rm s^{-1}}\,(T/10^4\ K)^{-0.507}(\nu/100\ {\rm GHz})^{0.118}\ D^2_{\rm Mpc}\ S_{3.3\ {\rm mm}}\,({\rm mJy})$. For a mean star-formation timescale of 5 Myr for the star formation, and for a radio continuum flux of ∼1 mJy for Cloud C (Meier et al. 2002), which contains most of the Streamer emission, the estimated mass depletion timescale is $\tau_{\rm dep} = M_{\rm gas}/{\rm star\text{-}formation\ rate\ (SFR)} \approx 0.3$ Gyr for the Streamer. We estimate that this number is uncertain to factors of 3–5, due to the unknown star-formation timescale and the uncertain gas mass.

The central 1″ (∼18.4 pc) region surrounding the supernebula, Cloud D, is forming stars at a SFR of $\sim 0.1\ M_\odot\ {\rm yr^{-1}}$ (Turner et al. 2015; Bendo et al. 2017). CO(2–1) images indicate that $M_{\rm H_2} \sim 8 \times 10^5\ M_\odot$ within Cloud D. If this gas is all associated with the current star formation, the gas depletion timescale is $\tau_{\rm SF} \sim 8$ Myr. However, these ALMA maps reveal that Cloud D actually consists of many clumps (Section 5), and it is unclear if all of them are related to the currently forming massive cluster. If some of this gas is not associated with the current star formation as suggested by the gas kinematics Turner et al. (2017), then this is an upper limit to $\tau_{\rm SF}$.

The molecular gas depletion time in the Streamer, $\tau_{\rm dep} = 0.3$ Gyr, is less than the median value of 0.8 Gyr for local low-metallicity galaxies as determined by Schruba et al. (2011), but within the observed spread. While CO-dark H_2 may be partly responsible for the low value, presumably the same holds for the general low-metallicity sample as a whole. It may also be that the ionized gas of the Streamer is caused by UV photons from the nuclear starburst, and not from star formation within the streamer, which would increase the value of $\tau_{\rm dep}$.

Cloud D has a very short molecular gas depletion time of $\tau_{\rm dep} = 8$ Myr, a factor of ∼100 times smaller than that of the typical low-metallicity galaxy in the Schruba et al. (2011) sample. We caution that the central gas mass is uncertain, and that the star-formation rate depends on our assumption of 5 Myr for the age; the latter is probably uncertain to factor two, although there is an additional uncertainty in the spread in star-formation age. However, these uncertainties of a factor of a few are not expected to be large enough to explain the two order of magnitude shorter depletion time in Cloud D1. This star formation is unusually efficient.

Lada et al. (2013) point out that individual GMCs in the galaxy do not obey a Kennicutt–Schmidt law; the star-formation rate surface density varies more than two orders of magnitude among Galactic GMCs. They propose that the Schmidt–Kennicutt law for galaxies (Kennicutt 1989, 1998) is a function of relative dense gas fraction and beam dilution on kpc scales. With these high-resolution ALMA images we resolve individual GMCs in NGC 5253, and thus it is not surprising that we see a spread in star-formation surface densities similar to that observed in Galactic GMCs. However by Galactic standards, Cloud D is extraordinarily efficient at forming stars.

5. Analysis of ^{13}CO in the Clumps within Cloud D

Images of the ^{12}CO(3–2) and ^{13}CO(3–2) for the central ∼100 pc region corresponding to Cloud D are shown in Figure 5. With the high ∼5 pc resolution of the ALMA images, the central Cloud D detected in the CO(3–2) images from the Submillimeter Array (Turner et al. 2015), breaks into a number of smaller clouds with diameters of ∼5–20 pc.

The larger CO structures are labeled and their characteristics are detailed in Table 1. ^{13}CO(3–2) emission provides valuable additional information on the optical depth of the CO and the gas mass in the central star-forming region of NGC 5253. All of the clouds in the central region are at least weakly detected in ^{13}CO. ^{13}CO(3–2) emission is also detected for the brighter clouds in the Streamer, not shown here; but this emission is very faint ($\lesssim 2\sigma$).

Clouds D3, D4, D5, D6, and Cloud F have ^{12}CO(3-2)/^{13}CO(3-2) flux ratios of ∼6–8. These values are somewhat lower than the value of ∼13 observed in Orion (Schilke et al. 1997). We infer that, as in Orion, these clouds are optically thick in ^{12}CO(3-2). In fact, half of the measured 2.4 Jy km s^{-1} of ^{13}CO(3-2) emission arises in Cloud D4, an apparently massive cloud in the central region located about 15–20 pc southwest of the supernebula that does not host obvious star formation and has an optically thick ^{12}CO/^{13}CO ratio of 7. Cloud D4 also appears in H_2 λ2.12 μm images of the region (Cresci et al. 2005), suggesting the presence of shocks (turbulence) or fluorescence; given the extinction implied by the CO, it is likely that the H_2 emission arises on the near surface of the cloud.

The highest ^{12}CO(3–2)/^{13}CO(3–2) ratio is ∼40 for Cloud D1, the small ($r \sim 2.8$ pc) cloud coincident with the giant

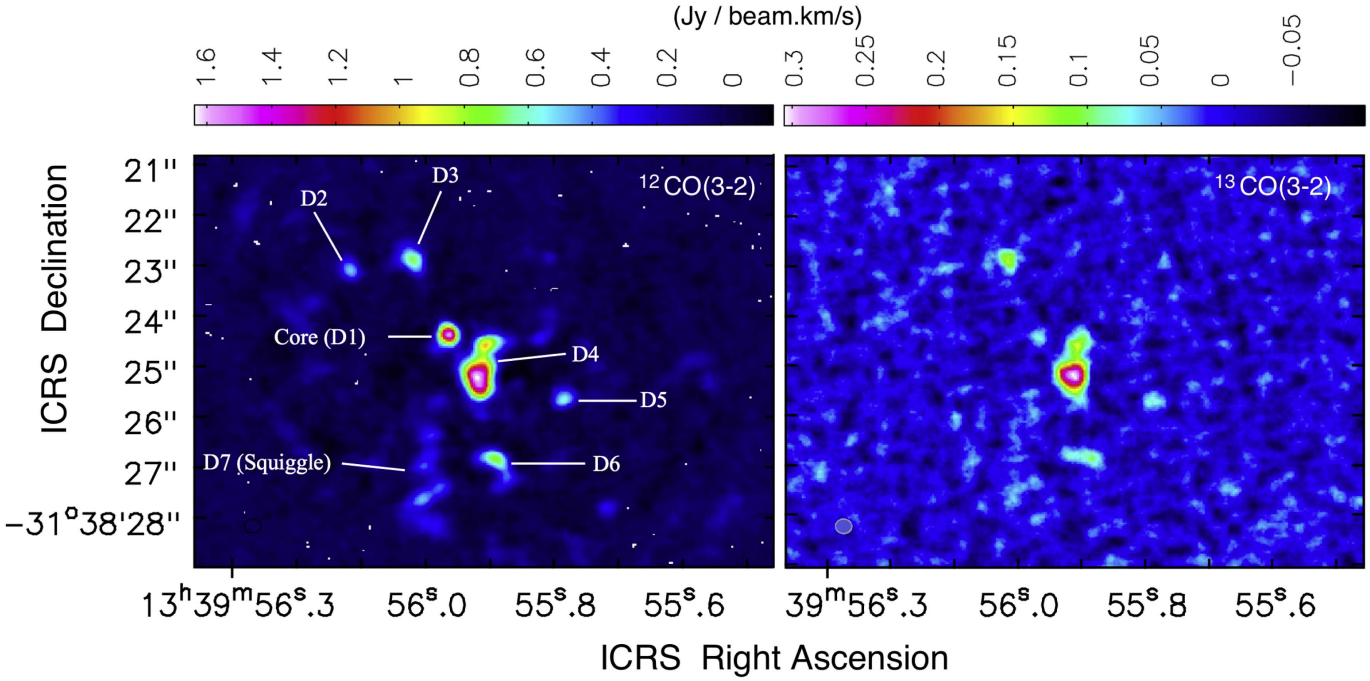

Figure 5. The central region (Cloud D). Left: the ALMA $0\farcs33 \times 0\farcs27$ ^{12}CO(3–2) map with the central regions labeled. rms in a 1 km s^{-1} channel is 2.7 mJy/bm. Right: the ALMA $0\farcs22 \times 0\farcs29$ ^{13}CO(3–2) map. rms in a 1 km s^{-1} channel is 3.3 mJy/bm.

central H II region known as the supernebula. This value is uncertain because the ^{13}CO(3–2) is so weak, but is unlikely to be < 20. Star formation may still be ongoing within Cloud D1, which appears to coexist with the $\sim 2.5 \times 10^5\ M_\odot$ SSC and H II region (Turner et al. 2017). Based on the high ^{12}CO(3–2)/^{12}CO(2–1) ratios of lower resolution maps, Turner et al. (2015) suggested that the larger Cloud D is optically thin. The ^{12}CO(3–2)/^{13}CO(3–2) ratio for Cloud D1 is consistent with the suggestion. This situation would be unusual; Galactic GMCs are optically thick in these lines. Cloud D1 may be optically thin because the gas is hot (Turner et al. 2015) and the molecules spread out over the rotational ladder. At 300 K, the partition function is 100, such that only 1% of the CO molecules will be in the ground state and ~3% in $J = 1$. It is also possible that Cloud D1 could also have selective photodissociation or that the ^{12}CO(3–2) and ^{13}CO(3–2) could probe different physical environments due to temperature gradients in cloud surfaces due to the presence of strong radiation fields in the cluster environment. Cloud D1 is also bright in H_2 $\lambda 2.12$ μm emission (Cresci et al. 2005); given that Cloud D1 is likely to consist of multiple star-forming clumps, the H_2 emission may arise on the surfaces of these individual clumps. (However Clouds D4 and D6, which are optically thick, are also bright in the H_2 line).

Cloud D2, located ~40 pc to the northeast of Cloud D1, may also be optically thin with a ^{12}CO/^{13}CO ratio of ~12, which is higher than average for this galaxy. As this cloud appears in radio continuum emission at cm wavelengths (Beck 2017, private communication) and in H_2 $\lambda 2.12$ μm emission (Cresci et al. 2005), Cloud D2 appears similar to Cloud D1, if smaller in scale. Thus, Cloud D2 appears to be a young, compact cluster that has warm molecular gas, although significantly smaller than that of the massive cluster within D1.

If ^{13}CO(3-2) is optically thin in some clouds, we can use the ^{13}CO integrated line intensities to estimate optically thin masses. These masses are given in Table 1. For Cloud D1 we adopt a temperature of 300 K, based on RADEX models of the CO(3–2)/CO(2–1) line ratio (Turner et al. 2015), and for clouds besides D1 we adopt 20 K. The optically thin masses are not very sensitive to temperature for this line until temperatures exceed ~100 K, although if the clouds are actually very warm, these masses will be underestimates. If we adopt a Galactic [CO]/[H_2] ratio of 8.5×10^{-5} and a [^{12}CO]/[^{13}CO] abundance ratio of 40, the minimum indicated by the Cloud D1 line ratio, we obtain cloud masses $M_{\rm Cl} \sim$ 0.6–11 $\times 10^3\ M_\odot$ (Table 1), with the most massive cloud being the apparently quiescent Cloud D4.

The masses based on ^{12}CO(3-2), assuming a conversion factor (^{12}CO Masses), and those based on ^{13}CO(3-2). assuming optically thin emission (^{13}CO Masses), differ by an order of magnitude. There are many possible reasons for the differences. For optically thin clouds, D1, D2, the values of [CO]/[H_2], and the [^{13}CO]/[^{12}CO] abundance ratios are sources of systemic uncertainty, since they may differ significantly from Galactic values in this low-metallicity galaxy. For optically thick clouds, the conversion factor cannot account for clouds that are unusually warm; or that have significant stellar mass contained within the cloud, such as Clouds D1 and D2; or for clouds that have significant CO-dark gas, although this is not likely to be a major mass contributor in these dense clouds (Langer et al. 2014).

The CO(3-2) critical density is aligned with the gas densities expected for star-forming gas. Even the highest estimates of cloud mass indicate that the gas masses of these clouds are fairly small. The largest cloud, D4, has an estimated mass of $3.4 \times 10^5\ M_\odot$, a relatively low mass considering the $\sim 10^5\ M_\odot$ star clusters that NGC 5253 has been forming. The current suite of clouds does not seem capable of forming a massive SSC, unless mergers of clouds take place, perhaps along accreting filaments, and if the star formation is extraordinarily efficient.

6. Summary and Conclusions

We present new ALMA images of ^{12}CO(3–2) and ^{13}CO(3–2) emission from the nearby (3.8 Mpc) dwarf galaxy NGC 5253. The spatial resolution is ∼0.″3, ten times smaller in diameter than that of the best previous maps. The images reveal dense (∼20,000 cm^{-3}) molecular clumps ∼5 pc in diameter with estimated masses of a few thousand $M_{\odot}$.

While atomic and ionized filaments are a feature of NGC 5253 on the largest scales (Kobulnicky & Skillman 2008), these observations are the first to detect clear, kinematically distinct filaments in the molecular gas. The inner 200 pc of NGC 5253 holds four filaments, composed of small (∼5 pc diameter) clouds. These filaments extend to ∼50–150 pc in length. The Streamer filament, detected previously in CO(1-0) and CO(2-1) in lower resolution images, is aligned along the prominent dust lane to the east of the galaxy. The Streamer is redshifted with respect to the systemic velocity, and thus appears to be falling into the galaxy. Also redshifted and in the foreground, thus apparently infalling, is the weaker Southern filament to the south of the galaxy center. Cloud F, a filament southwest of the center, is blueshifted with respect to the galaxy but shows no apparent extinction and may be on the far side of the galaxy. We propose that the CO filaments form the inner position of H I filaments that are falling into the galaxy from outside. This model particularly explains the Streamer along the prominent dust lane (redshifted) and Cloud F (blueshifted, with no apparent foreground extinction). The clearest filaments have length-to-width aspect ratios of ≈20. Dense clumps in the filaments are likely to be overpressured relative to ambient gas, and probably gravitationally supported; they may be likely sites of future star formation.

The central cloud surrounding the supernebula, Cloud D, previously detected as a bright CO(3–2) source, breaks up into multiple clouds. Some of these clouds are optically thin in CO(3-2), as indicated by high ^{12}CO/^{13}CO flux ratios of ∼12–40, higher than the average cloud ratio of ∼6–8. Cloud D1 is coincident with the giant H II region and supernebula; its flux ratio of ^{12}CO/^{13}CO ∼ 40 suggests that the [^{12}CO]/[^{13}CO] ratio in NGC 5253 is $\gtrsim$40. Cloud D2 appears to contain a smaller young cluster. We propose that Clouds D1 and D2 are most likely optically thin in CO(3–2) because the molecular gas is hot, due to the proximity of young and massive star clusters, although it is also possible that optical depth effects in the presence of high temperature gradients could produce the high observed ratios. These clouds are likely to be brighter than would be expected based on their gas columns alone.

From radio continuum flux densities and lower J CO lines, we derive average gas depletion timescales of 0.3 Gyr for the Streamer and 8 Myr for Cloud D1 coincident with the supernebula. The masses we obtain for the individual clumps from the ALMA observations, from assumption of optically thin emission, for the thin clouds, and from ^{12}CO(3–2) emission, for the thick clouds, differ by about an order of magnitude. Uncertainties in the H_2 masses are due to unknown [CO]/[H_2] for this low metallicity, high radiation environment, unknown CO(3–2)/CO(1–0) ratio, and uncertainty in the conversion factor applicability. However, even the highest estimates of mass for the clumps,∼10^4–10^5 $M_{\odot}$, are small compared to the masses of the star clusters that are currently forming. This suggests that filament mergers and/or highly efficient star formation is taking place in NGC 5253. Further high-resolution CO observations may clarify these issues and allow for improved masses. Even with these uncertainties, it appears that the star formation in the central Cloud D1 associated with the supernebula is extraordinarily efficient.

This paper makes use of the following ALMA data: ADS/JAO.ALMA# 2012.1.00105.S. ALMA is a partnership of the ESO (representing its member states), NSF (USA), and NINS (Japan), together with NRC (Canada), *MOST*, ASIAA (Taiwan), and KASI (Republic of Korea), in cooperation with the Republic of Chile. The Joint ALMA Observatory is operated by the ESO, AUI/NRAO, and NAOJ. The National Radio Astronomy Observatory (NRAO) is a facility of the National Science Foundation operated under cooperative agreement by Associated Universities, Inc. Support for this work was provided by the NSF through award GSSP SOSPA2-016 from the NRAO to S.M.C. and grant AST 1515570 to J.L.T., and by the UCLA Academic Senate through a COR seed grant. The authors wish to thank W. M. Goss, P. T. P. Ho, and the anonymous referee for their helpful comments.

Facility: ALMA.

ORCID iDs

S. Michelle Consiglio https://orcid.org/0000-0002-0214-0491
Jean L. Turner https://orcid.org/0000-0003-4625-2951
Sara Beck https://orcid.org/0000-0002-5770-8494
David S. Meier https://orcid.org/0000-0001-9436-9471
Sergiy Silich https://orcid.org/0000-0002-3814-5294
Jun-Hui Zhao https://orcid.org/0000-0002-1317-3328

References

Alonso-Herrero, A., Takagi, T., Baker, A. J., et al. 2004, ApJ, 612, 222
Atherton, P. D., Taylor, K., Pike, C. D., et al. 1982, MNRAS, 201, 661
Bendo, G. J., Miura, R. E., Espada, D., et al. 2017, MNRAS, 472, 1239
Bisbas, T. G., Papadopoulos, P. P., & Viti, S. 2015, ApJ, 803, 37
Burbidge, E. M., & Burbidge, G. R. 1962, ApJ, 135, 694
Caldwell, N., & Phillips, M. M. 1989, ApJ, 338, 789
Calzetti, D., Harris, J., Gallagher, J. S., III, et al. 2004, AJ, 127, 1405
Calzetti, D., Johnson, K. E., Adamo, A., et al. 2015, ApJ, 811, 75
Calzetti, D., Meurer, G. R., Bohlin, R. C., et al. 1997, AJ, 114, 1834
Consiglio, S. M., Turner, J. L., Beck, S., & Meier, D. S. 2016, ApJL, 833, L6
Cresci, G., Vanzi, L., & Sauvage, M. 2005, A&A, 433, 447
de Grijs, R., Anders, P., Zackrisson, E., & Östlin, G. 2013, MNRAS, 431, 2917
Gorjian, V. 1996, AJ, 112, 1886
Gorjian, V., Turner, J. L., & Beck, S. C. 2001, ApJL, 554, L29
Graham, J. A. 1981, PASP, 93, 552
Heiderman, A., Evans, N. J., II, Allen, L. E., Huard, T., & Heyer, M. 2010, ApJ, 723, 1019
Hunt, L., Bianchi, S., & Maiolino, R. 2005, A&A, 434, 849
Inoue, A. K. 2001, AJ, 122, 1788
Kennicutt, R. C., Jr. 1989, ApJ, 344, 685
Kennicutt, R. C., Jr. 1998, ApJ, 498, 541
Kobulnicky, H. A., & Skillman, E. D. 1995, ApJL, 454, L121
Kobulnicky, H. A., & Skillman, E. D. 2008, AJ, 135, 527
Koribalski, B. S., Staveley-Smith, L., Kilborn, V. A., et al. 2004, AJ, 128, 16
López-Sánchez, Á. R., Koribalski, B. S., van Eymeren, J., et al. 2012, MNRAS, 419, 1051
Lada, C. J., Lombardi, M., & Alves, J. F. 2010, ApJ, 724, 687
Lada, C. J., Lombardi, M., Roman-Zuniga, C., Forbrich, J., & Alves, J. F. 2013, ApJ, 778, 133
Langer, W. D., Velusamy, T., Pineda, J. L., Willacy, K., & Goldsmith, P. F. 2014, A&A, 561, A122
Lombardi, M., Alves, J., & Lada, C. J. 2010, A&A, 519, L7
Lundgren, A., Leon, S., Hibbard, J., Müller, E., & Di Francesco, J. 2013, ALMA Technical Handbook Version 1.1, ALMA (Garching: ESO)
Mac Low, M.-M., & Ferrara, A. 1999, ApJ, 513, 142
Martin, C. L. 1998, ApJ, 506, 222
Martín-Hernández, N. L., Schaerer, D., & Sauvage, M. 2005, A&A, 429, 449

Meier, D. S., Turner, J. L., & Beck, S. C. 2002, AJ, 124, 877
Meier, D. S., Turner, J. L., Crosthwaite, L. P., & Beck, S. C. 2001, AJ, 121, 740
Meurer, G. R., Heckman, T. M., Leitherer, C., et al. 1995, AJ, 110, 2665
Miura, R. E., Espada, D., Sugai, H., Nakanishi, K., & Hirota, A. 2015, PASJ, 67, L1
Rosolowsky, E., & Leroy, A. 2006, PASP, 118, 590
Sakai, S., Ferrarese, L., Kennicutt, R. C., Jr., & Saha, A. 2004, ApJ, 608, 42
Schilke, P., Groesbeck, T. D., Blake, G. A., & Phillips, T. G. 1997, ApJS, 108, 301
Schruba, A., Leroy, A. K., Walter, F., et al. 2011, AJ, 142, 37
Smith, L. J., Crowther, P. A., Calzetti, D., & Sidoli, F. 2016, ApJ, 823, 38
Tremonti, C. A., Calzetti, D., Leitherer, C., & Heckman, T. M. 2001, ApJ, 555, 322
Turner, J. L., & Beck, S. C. 2004, ApJL, 602, L85
Turner, J. L., Beck, S. C., Benford, D. J., et al. 2015, Natur, 519, 331
Turner, J. L., Beck, S. C., Crosthwaite, L. P., et al. 2003, Natur, 423, 621
Turner, J. L., Beck, S. C., & Ho, P. T. P. 2000, ApJL, 532, L109
Turner, J. L., Beck, S. C., & Hurt, R. L. 1997, ApJL, 474, L11
Turner, J. L., Consiglio, S. M., Beck, S. C., et al. 2017, ApJ, 846, 73
Turner, J. L., Ho, P. T. P., & Beck, S. C. 1998, AJ, 116, 1212
Vanzi, L., & Sauvage, M. 2004, A&A, 415, 509
Wolfire, M. G., McKee, C. F., Hollenbach, D., & Tielens, A. G. G. M. 2003, ApJ, 587, 278
Zastrow, J., Oey, M. S., Veilleux, S., McDonald, M., & Martin, C. L. 2011, ApJL, 741, L17